GEOLOGY | THE GEOLOGICAL SOCIETY OF AMERICA®

https://doi.org/10.1130/G47377.1

Manuscript received 10 January 2020
Revised manuscript received 17 March 2020
Manuscript accepted 22 March 2020

Published online 18 May 2020

Late Ordovician mass extinction caused by volcanism, warming, and anoxia, not cooling and glaciation

David P.G. Bond[1] and Stephen E. Grasby[2]
[1]Department of Geography, Geology and Environment, University of Hull, Hull HU6 7RX, UK
[2]Geological Survey of Canada, Natural Resources Canada, 3303 33rd Street NW, Calgary, Alberta T2L 2A7, Canada

ABSTRACT

The Ordovician saw major diversification in marine life abruptly terminated by the Late Ordovician mass extinction (LOME). Around 85% of species were eliminated in two pulses 1 m.y. apart. The first pulse, in the basal Hirnantian, has been linked to cooling and Gondwanan glaciation. The second pulse, later in the Hirnantian, is attributed to warming and anoxia. Previously reported mercury (Hg) spikes in Nevada (USA), South China, and Poland implicate an unknown large igneous province (LIP) in the crisis, but the timing of Hg loading has led to different interpretations of the LIP-extinction scenario in which volcanism causes cooling, warming, or both. We report close correspondence between Hg, Mo, and U anomalies, declines in enrichment factors of productivity proxies, and the two LOME pulses at the Ordovician-Silurian boundary stratotype (Dob's Linn, Scotland). These support an extinction scenario in which volcanogenic greenhouse gases caused warming around the Katian-Hirnantian boundary that led to expansion of a preexisting deepwater oxygen minimum zone, productivity collapse, and the first LOME pulse. Renewed volcanism in the Hirnantian stimulated further warming and anoxia and the second LOME pulse. Rather than being the odd-one-out of the "Big Five" extinctions with origins in cooling, the LOME is similar to the others in being caused by volcanism, warming, and anoxia.

INTRODUCTION

Ordovician Earth experienced major diversification in the oceans (Sepkoski, 1981), abruptly terminated by the first of the "Big Five" extinctions—the Late Ordovician mass extinction (LOME). Two pulses eliminated 85% of marine species (Fig. 1; Jablonski, 1991) during the second-most ecologically severe Phanerozoic crisis (Bambach et al., 2004). Extinction scenarios invoke changes in ocean temperature and redox chemistry: the first pulse in the basal Hirnantian affected nekton and plankton and has been linked to cooling at the onset of Gondwanan glaciation (Brenchley et al., 2001); a million years later, the second pulse in the latest Hirnantian accompanied warming, sea-level rise, and anoxia (Fig. 1; Nielsen, 2004). The link to cooling makes the LOME an outlier amongst the "Big Five": the other four are associated with large igneous province (LIP) volcanism and global warming (Bond and Wignall, 2014; Bond and Grasby, 2017). The ultimate driver of the LOME is unclear, but mercury (Hg) spikes (a volcanism proxy; see Grasby et al., 2019) in Ordovician–Silurian strata in Nevada (USA), South China, and Poland implicate a hitherto-undiscovered (or long-subducted) LIP (Gong et al., 2017; Jones et al., 2017; Smolarek-Lach et al., 2019). The timing of Hg-loading events—albeit based on sparse records—has led to different LIP-extinction models. The Jones et al. (2017) record from Nevada and South China sees episodes of Hg enrichment (diachronous between these regions) in pre-extinction Katian strata and in the mid-Hirnantian, before the second extinction pulse (Fig. 1). They suggested that chemical weathering of a Katian LIP drove Gondwanan cooling and extinction, while LIP activity in the Hirnantian resulted in a glacial maximum caused by the albedo effects of sulfate aerosols. The temporal scale of such climatic changes is at odds with the brevity of the two LOME pulses, and that the second pulse has been linked to warming is problematic for the Jones et al. (2017) model. The short atmospheric residence time of SO_2 makes its cooling effects minor compared to CO_2-driven warming, and modeling suggests that cooling resulting from LIP volcanism is an unlikely extinction driver (Schmidt et al., 2016).

In their South China record, Gong et al. (2017) showed an increase in Hg from background levels of ~1 ppb to ~100 ppb coincident with a Katian facies change from limestone to shale. The ratio of Hg to total organic carbon (TOC) remains high (50–200 ppb/%) into the Silurian, with highest values coincident with the LOME pulses (Fig. 1). Gong et al. (2017) implicated the more geologically rapid effects of volcanism, such as metal toxicity, warming, ocean acidification, and anoxia. Confusingly, Katian to Hirnantian strata of Poland contain multiple Hg/TOC spikes (to 400–500 ppb/%), but none coincide with extinctions, and the greatest anomaly is mid-Katian, before the first LOME pulse (Smolarek-Lach et al., 2019). Discounting the LIP-LOME hypothesis, Shen et al. (2019) concluded that Hg in marine strata in South China is sulfide hosted and nonvolcanic. However, Hg stable isotopic evidence indicates a volcanic source (Gong et al., 2017). Whatever the source, there is evidence for widespread Hg loading during the LOME interval. Further Hg records are required in order to tease apart their spatial and temporal variability.

MATERIAL AND METHODS

Dob's Linn (UK; Fig. 2; 55°25′46.484″N, 3°16′17.605″W, North American Datum of 1983) is the stratotype for the base of the Silurian (443.8 ± 1.5 Ma). The succession records deepwater graptolitic shales and mudstones from a tropical (30°S) continental margin facing the Iapetus Ocean at the southern edge of Laurentia (Scotese and McKerrow, 1990). The dry United Kingdom summer of 2018 allowed sampling of normally underwater outcrops in the south bank of Linn Branch stream (Fig. 2) that provides a more complete, less faulted, less weathered, and previously unstudied expression of the north-bank stratotype. After removing weathered surfaces, we collected 62 samples (seven bentonites) from 2-cm-thick layers

CITATION: Bond, D.P.G., and Grasby, S.E., 2020, Late Ordovician mass extinction caused by volcanism, warming, and anoxia, not cooling and glaciation: Geology, v. 48, p. 777–781, https://doi.org/10.1130/G47377.1

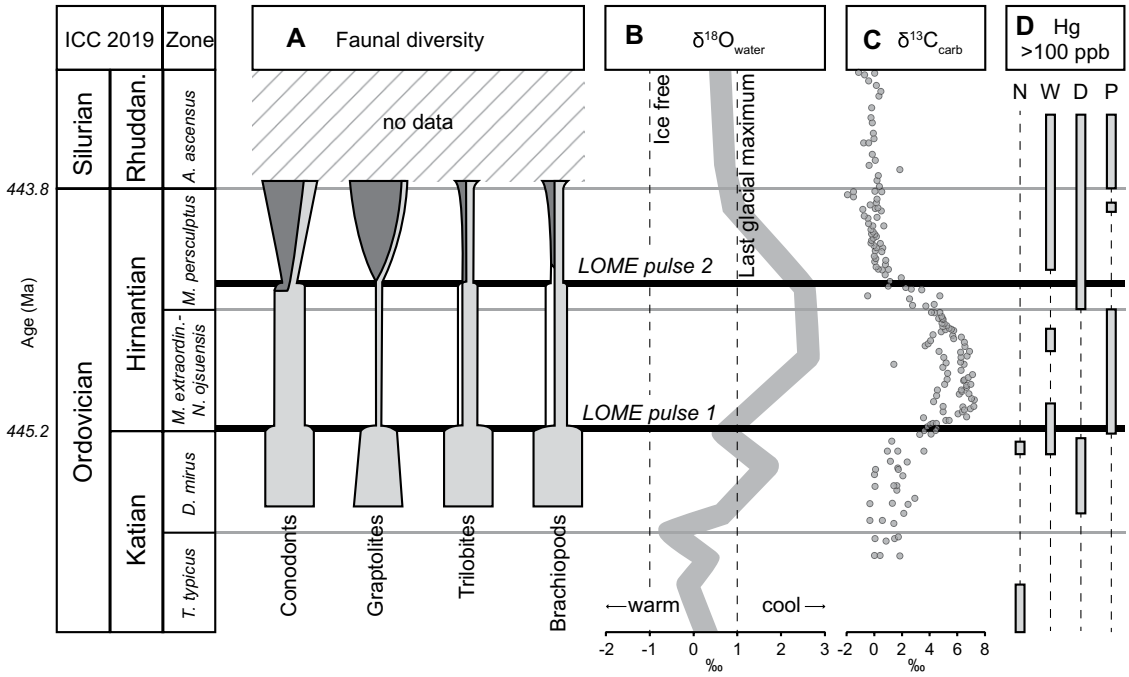

Figure 1. Global features of Late Ordovician mass extinction (LOME). (A) Faunal diversity (Brenchley et al., 2001) including pre-extinction biota (light gray), appearances post–LOME pulse 1 (white), and appearances post–LOME pulse 2 (dark gray). Width gives qualitative sense of within-group diversity changes. (B) $\delta^{18}O$ curve (Finnegan et al., 2011). First LOME pulse occurs at end of phase of warming. (C) Carbonate $\delta^{13}C$ ($\delta^{13}C_{carb}$) records from Laurentia (Kump et al., 1999; LaPorte et al., 2009), which indicate disturbance in carbon cycle associated both LOME pulses. (D) Range of Hg anomalies >100 ppb from Nevada (USA) (N), South China (W—Wangjiawan; D—Dingjiapo), and Poland (P) (Gong et al., 2017; Jones et al., 2017; Smolarek-Lach et al., 2019). Ages (in Ma) from International Chronostratigraphic Chart version 2019/05 (ICC 2019). Rhuddan.—Rhuddanian. Zone refers to graptolite zones (genus abbreviations: *T.* = *Tangyagraptus*; *D.* = *Dicellograptus*; *M.* = *Metabolograptus*; *N.* = *Normalograptus*; *A.* = *Akidograptus*).

through 25.5 m of the Upper Hartfell Shale and the Birkhill Shale. We collected 10 further samples at the stratotype itself (55°25′46.799″N, 3°16′16.977″W) to fill a 2 m gap at the top of the Upper Hartfell Shale (poorly exposed in our main section).

In the laboratory, fresh samples were powdered by agate mortar and pestle. We generated an organic $\delta^{13}C$ ($\delta^{13}C_{org}$) curve to facilitate global correlation. Samples were washed with HCl and decarbonated with hot distilled water. $\delta^{13}C$ was measured using continuous flow–elemental analysis–isotope ratio mass spectrometry with a Finnigan Mat Delta^{plus}XL mass spectrometer interfaced with a Costech 4010 elemental analyzer with combined analytical and sampling error of ±0.2‰. Samples were subjected to trace metal assays at the Geological Survey of Canada (Calgary, Alberta), where powdered material digested in a 2:2:1:1 acid solution of H_2O-HF-$HClO_4$-HNO_3 was analyzed using a PerkinElmer mass spectrometer with ±2% analytical error, and we use redox-sensitive trace metals Mo and U (normalized to Al) and Mn as proxies for oxygenation. Trace metals that act as micronutrients can be used as proxies for paleoproductivity (Tribovillard et al., 2006), but because no single element is reliable, we use concentrations of Ba, Ni, P, and Zn, calculating element enrichment factors (EFs) for these as deviations of Al-normalized samples (to account for terrestrial input) from post-Archean average ahale values (PAAS; Wedepohl, 1995). Enrichment factors >1, calculated as $EF = (X_{sample}/Al_{sample})/(X_{PAAS}/Al_{PAAS})$, indicate high primary productivity (Tribovillard et al., 2006). We measured Hg concentrations using a LECO AMA254 mercury analyzer. We normalized Hg to total Al (from mass spectrometry) and TOC measured using HAWK pyrolysis, with ±5% analytical error of reported value, based on repeats and reproducibility of standards run after every fifth sample (Lafargue et al., 1998). Hg was normalized to TOC only where the latter concentrations are >0.2% because normalizing to smaller values magnifies errors unacceptably (e.g., Grasby et al., 2016).

RESULTS

Our $\delta^{13}C_{org}$ curve accords with published records and shows a positive trend from −33‰ to −27‰ in the Katian prior to a minor negative shift to ~−30‰ (Fig. 3). Values stabilize between

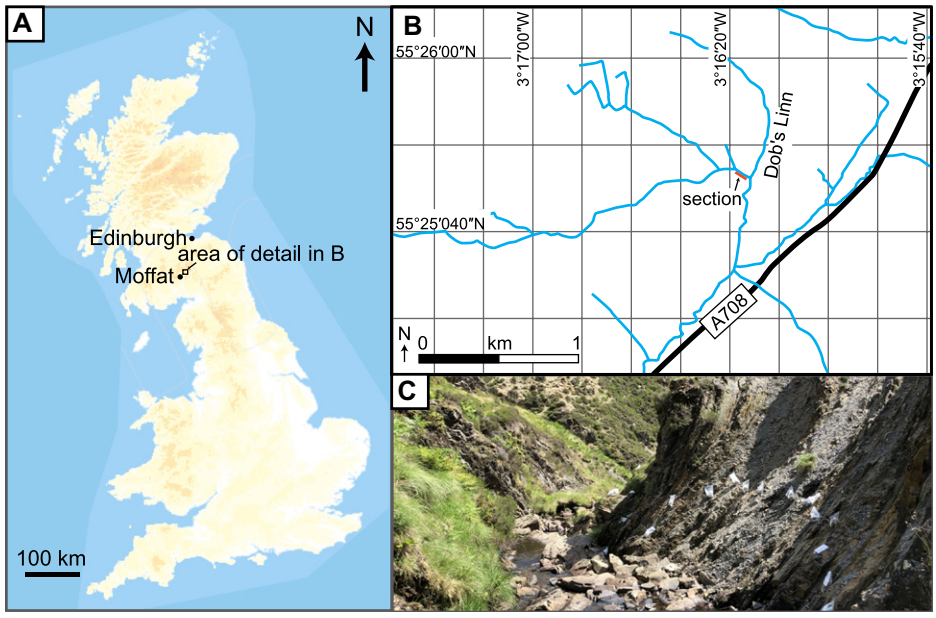

Figure 2. Maps (A—Great Britain; B—section location) and photograph (C) of Dob's Linn (Scotland, UK; 55°25′46.484″N, 3°16′17.605″W, North American Datum of 1983). View is to the southeast. Sample bags in C are 20 cm long.

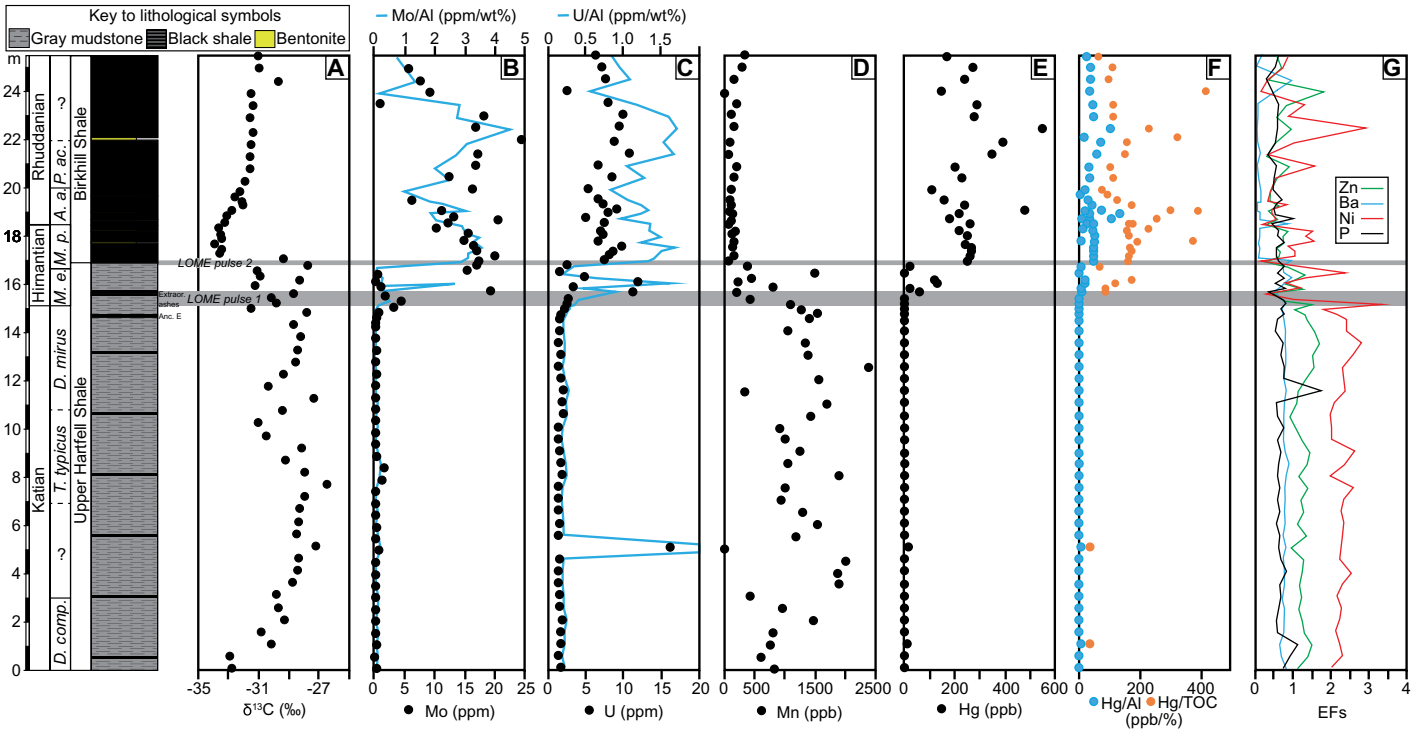

Figure 3. Geochemical data from Dob's Linn (Scotland, UK). (A) Organic $\delta^{13}C$ ($\delta^{13}C_{org}$). (B) Mo and Mo/Al. (C) U and U/Al. (D) Mn. (E) Hg. (F) Hg normalized to total organic carbon (TOC) and total Al. (G) Enrichment factors (EFs) of Zn, Ba, Ni, and P. "ashes" marks level at which numerous thin ash beds appear. Graptolite zonation based on Williams (1988), Rong et al. (2008), and Zhou et al. (2015): *D. comp.—Dicellograptus complexus*; *T. typicus—Tangyagraptus typicus*; *D. mirus—Dicellograptus mirus*; *M. e.—Metabolograptus extraordinarius–Normalograptus ojsuensis*; *M. p.—Metabolograptus persculptus*; *A. a.—Akidograptus ascensus*; *P. ac.—Parakidograptus acuminatus*. Graptolite bands: Anc. E—Anceps Band E; Extraor.—Extraordinarius Band.

~–31‰ and –28‰ to the top of the Upper Hartfell Shale in the Hirnantian. The base of the Birkhill Shale sees a negative $\delta^{13}C_{org}$ excursion from –29.4‰ to –33.6‰, above which values recover to ~–31‰ at the section top.

Concentrations of Mo and U and their Al-normalized values are low (generally <1 ppm and <2 ppm respectively) through the Upper Hartfell Shale to 15 m. Mn concentrations are generally between 500 ppm and 2000 ppm in this interval. Mo and U concentrations rise and Mn concentrations fall—modestly at first, and then by an order of magnitude—between *Anceps* (graptolite) Band E at 14.7 m and the *Extraordinarius* Band at 15.6 m (first LOME pulse). Intriguingly, numerous centimeter-thick ash beds appear at this level. Concentrations of Mo and U rise dramatically at the base of the Birkhill Shale at 16.9 m (second LOME pulse) to ~20 ppm and 10 ppm respectively, and when normalized to Al, these elements remain enriched into the Rhuddanian. Mn concentrations covary inversely with Mo and U, falling away to values in the low hundreds of parts per million in the Birkhill Shale (Fig. 3).

Three of our paleoproductivity proxies (Ba, P, and Zn) have EFs of ~1 in much of the Upper Hartfell Shale, while Ni is highly enriched with EFs of 2–3.5. The EFs of all four drop between *Anceps* Band E and the *Extraordinarius* Band (first LOME pulse) to ~0.5 (Ni falls from its highest EF value of 3.5). The EFs of Ba, Ni, and Zn fall close to 0 at the base of the Birkhill Shale (second LOME pulse). The EFs of all four elements are consistently lower in the Birkhill Shale than in pre-extinction strata of the Upper Hartfell Shale (Fig. 3).

Mercury concentrations are at or below the limit of detection (10 ppb) through most of the Upper Hartfell Shale, exceeding this value in its upper meter, within the *Extraordinarius* Band where Hg reaches 60 ppb and in the overlying 60 cm of mudstone with thin ash beds (Hg up to 130 ppb). Hg concentrations increase dramatically at the base of the Birkhill Shale (second LOME pulse) to ~200–300 ppb and peak at 550 ppb in the early Rhuddanian (Fig. 3). These spikes withstand normalization to TOC and total Al, suggesting that they reflect increased Hg flux to the system rather than enhanced sequestration under anoxic conditions. Geochemical data are available in Table S1 in the Supplemental Material[1].

EXTINCTION SCENARIO

Redox-sensitive trace metals suggest that both LOME pulses are associated with episodes of dysoxic or anoxic conditions (the second being more intense and persistent) separated by a period of reoxygenation. Anoxia is a potent killer that can account for extinctions in benthic groups and deeper-dwelling graptolites and conodonts. This is at odds with the long-standing view linking the first pulse to cooling and glaciation (Sheehan, 1973; Brenchley et al., 2001) at a time of sea-level fall because anoxia is a function of warming. We cannot fully resolve this dichotomy but note that numerous records (summarized by Haq and Schutter [2008]) imply sea-level fall at the Katian-Hirnantian boundary, coincident with the onset of the first LOME pulse, but that this pulse continued into the earliest Hirnantian by which time sea-level was already rising. Furthermore, the timing of the Gondwanan glaciation that purportedly drove sea-level fall is controversial: it probably commenced before the Hirnantian and continued into the Silurian (Díaz-Martínez and Grahn, 2007; Finnegan et al., 2011; Nardin et al., 2011). Such a long-lived phenomenon is inconsistent with the abruptness of both extinction pulses. Finnegan et al.'s (2011) oxygen isotope curve (Fig. 1) reveals that the first LOME pulse occurred at the end of a warming phase as $\delta^{18}O$ shifted from +2‰ to ~+0.5‰. An anoxic water mass probably lurked close by during much of the pre-extinction interval at Dob's Linn, a not-uncommon phenomenon in early Paleozoic oceans where dissolved O_2

[1]Supplemental Material. Geochemical data from the Dob's Linn section (Scotland, UK). Please visit https://doi.org/10.1130/GEOL.26213S.12221825 to access the supplemental material, and contact editing@geosociety.org with any questions.

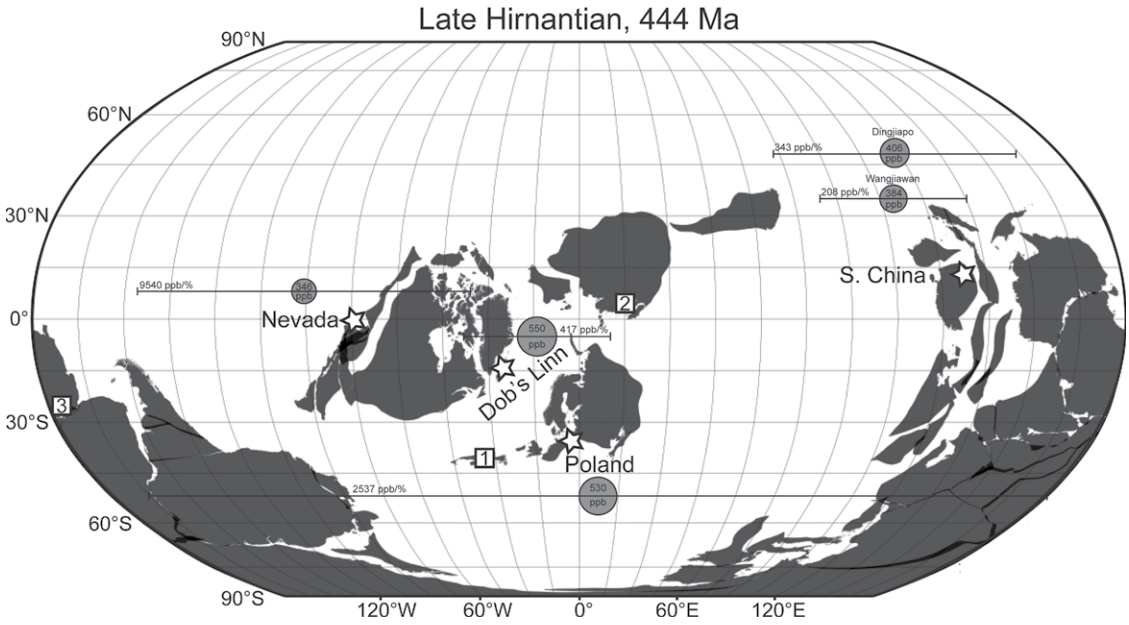

Figure 4. Late Hirnantian (444 Ma) paleogeography (GPlates PALEOMAP model; https://www.gplates.org/) with sites (stars) of known Hg anomalies (gray circles scaled to maximum Hg concentrations; whiskers scaled to maximum Hg to total organic carbon [TOC] ratio). We exclude value of 2964 ppb Hg in Nevada (USA) that Jones et al. (2017) term "upper *pacificus* anomaly", and their Hg/TOC peak of 9540 ppb/% is function of normalizing to TOC of 0.04% (whisker has been shortened by factor of 20 relative to other sites; likewise Poland whisker has been halved in length). Maximum Hg concentrations in Poland (530 ppb) and at Dob's Linn (Scotland, UK; 550 ppb) are from Rhuddanian shales. Sites of volcanism (white squares): 1—Cape St. Mary's, Newfoundland, Canada; 2—Suordakh, Siberia, Russia; 3—Sierra del Tigre, Argentina.

was less than half that of modern oceans (Bergman et al., 2004; Dahl et al., 2010). Thus, Katian strata are enriched in Mn, invoking the "bath tub ring" effect whereby Mn(II) is soluble in anoxic waters but precipitates where the redox boundary intercepts the seafloor (Frakes and Bolton, 1984). Our Mn record implies that anoxia developed in deeper parts of the basin during the Katian, and when this expanded upslope, it drove the first LOME pulse. This is supported by a widespread positive excursion in $\delta^{34}S$ of pyrite sulfur in the earliest Hirnantian suggestive of the global expansion of euxinia (Hammarlund et al., 2012). The second LOME pulse is oft linked to anoxia due to the facies change at the base of the Birkhill Shale, and our redox proxies support this. Thus, as persistently oxygen-poor conditions established, Mn was no longer sequestered into sediment, leading to an inverse relationship between (1) Mn and (2) Mo and U. Our trace metal data suggest that these anoxic pulses were separated by a better-oxygenated interval, coinciding with cooling inferred from Finnegan et al.'s (2011) oxygen isotope data.

The decline in EFs in our productivity proxies suggest that the first and especially second LOME pulses were associated with a collapse in primary productivity. This is consistent with the nitrogen isotope record from Dob's Linn, where $\delta^{15}N$ hovers at ~0‰ through the Hirnantian, indicating persistent limitation of fixed nitrogen throughout the LOME interval (Koehler et al., 2019). The collapse in productivity during the first LOME pulse might have been global—the Nanbazi section in South China records a fall in biogenic Ba from ~400 ppm to values close to 0 ppm across the Katian-Hirnantian boundary (Zhou et al., 2015).

Our Hg record suggests that the expansion of anoxia and productivity collapse coincided with the onset of volcanism. A negative shift in the $\delta^{7}Li$ record initiates 3 m below the Ordovician-Silurian boundary at Dob's Linn—precisely the level of the first LOME pulse (Pogge von Strandmann et al., 2017)—and may reflect enhanced continental weathering driven by volcanically induced environmental change. The appearance of numerous thin ash beds at the level of the first LOME pulse suggests that the site of volcanism might have been proximal. Hg spikes are now known from the LOME interval from opposite margins of Laurentia, Baltica, and South China (Fig. 4), but this study is the first to link Hg enrichments directly to both extinction pulses. The largest known Hg anomalies occur at Dob's Linn (550 ppb) and Poland (530 ppb; Smolarek-Lach et al., 2019; Fig. 4), perhaps suggesting that these were closest to the site of volcanism. The Cape St. Mary's sills of Newfoundland (Canada) and the Suordakh intraplate event in eastern Siberia (Russia) are candidate LIP remnants (Gong et al., 2017; Jones et al., 2017; Fig. 4), but further dating work is required to evaluate these.

CONCLUSIONS

The correspondence between Hg, Mo, and U anomalies, declines in EFs of productivity proxies, and the two LOME pulses at Dob's Linn support a volcanically driven extinction scenario in which greenhouse gases from potentially LIP-scale eruptions caused global warming around the Katian-Hirnantian boundary. This led to the expansion of a preexisting deepwater oxygen minimum zone that may have resulted in productivity collapse and the first LOME pulse among benthic groups and deep-dwelling plankton and nekton. Survivors struggled through the Hirnantian as climate cooled and the anoxic water mass retreated to the deeper basin. This amelioration was temporary, and a million years later, renewed volcanism stimulated further warming, intensified anoxia, and the second LOME pulse. For many years, the LOME was considered unlike the other "Big Five" extinctions—being associated with cooling and with no obvious trigger—but it now appears that this, like every major Phanerozoic crisis, was caused by volcanism, warming, and anoxia. The removal of cooling from the list of Phanerozoic extinction drivers has relevance to the modern phase of global warming: rather than casting doubt on the warming-extinction nexus, the LOME now corroborates it. All major mass extinctions are associated with global warming.

ACKNOWLEDGMENTS

This study received funding from UK Natural Environment Research Council grant NE/J01799X/1 to Bond.

REFERENCES CITED

Bambach, R.K., Knoll, A.H., and Wang, S.C., 2004, Origination, extinction, and mass depletions of marine diversity: Paleobiology, v. 30, p. 522–542, https://doi.org/10.1666/0094-8373(2004)030<0522:OEAMDO>2.0.CO;2.

Bergman, N.M., Lenton, T.M., and Watson, A.J., 2004, COPSE: A new model of biogeochemical cycling over Phanerozoic time: American Journal of Science, v. 304, p. 397–437, https://doi.org/10.2475/ajs.304.5.397.

Bond, D.P.G., and Grasby, S.E., 2017, On the causes of mass extinctions: Palaeogeography, Palaeoclimatology, Palaeoecology, v. 478, p. 3–29, https://doi.org/10.1016/j.palaeo.2016.11.005.

Bond, D.P.G., and Wignall, P.B., 2014, Large igneous provinces and mass extinctions: An update, *in* Keller, G., and Kerr, A.C., eds.,

Volcanism, Impacts, and Mass Extinctions: Causes and Effects: Geological Society of America Special Paper 505, p. 29–55, https://doi.org/10.1130/2014.2505(02).

Brenchley, P.J., Marshall, J.D., and Underwood, C.J., 2001, Do all mass extinctions represent an ecological crisis? Evidence from the Late Ordovician: Geological Journal, v. 36, p. 329–340, https://doi.org/10.1002/gj.880.

Dahl, T.W., Hammarlund, E.U., Anbar, A.D., Bond, D.P.G., Gill, B.C., Gordon, G.W., Knoll, A.H., Nielsen, A.T., Schovsbo, N.H., and Canfield, D.E., 2010, Devonian rise in atmospheric oxygen correlated to the radiations of terrestrial plants and large predatory fish: Proceedings of the National Academy of Sciences of the United States of America, v. 107, p. 17,911–17,915, https://doi.org/10.1073/pnas.1011287107.

Díaz-Martínez, E., and Grahn, Y., 2007, Early Silurian glaciation along the western margin of Gondwana (Peru, Bolivia and northern Argentina): Palaeogeographic and geodynamic setting: Palaeogeography, Palaeoclimatology, Palaeoecology, v. 245, p. 62–81, https://doi.org/10.1016/j.palaeo.2006.02.018.

Finnegan, S., Bergmann, K., Eiler, J.M., Jones, D.S., Fike, D.A., Eisenman, I., Hughes, N.C., Tripati, A.K., and Fischer, W.W., 2011, The magnitude and duration of Late Ordovician–Early Silurian glaciation: Science, v. 331, p. 903–906, https://doi.org/10.1126/science.1200803.

Frakes, L.A., and Bolton, B.R., 1984, Origin of manganese giants: Sea-level change and anoxic-oxic history: Geology, v. 12, p. 83–86, https://doi.org/10.1130/0091-7613(1984)12<83:OOMGSC>2.0.CO;2.

Gong, Q., Wang, X., Zhao, L., Grasby, S.E., Chen, Z.-Q., Zhang, L., Li, Y., Cao, L., and Li, Z., 2017, Mercury spikes suggest volcanic driver of the Ordovician-Silurian mass extinction: Scientific Reports, v. 7, 5304, https://doi.org/10.1038/s41598-017-05524-5.

Grasby, S.E., Beauchamp, B., Bond, D.P.G., Wignall, P.B., and Sanei, H., 2016, Mercury anomalies associated with three extinction events (Capitanian Crisis, Latest Permian Extinction and the Smithian/Spathian Extinction) in NW Pangea: Geological Magazine, v. 153, p. 285–297, https://doi.org/10.1017/S0016756815000436.

Grasby, S.E., Them, T.R., II, Chen, Z., Yin, R., and Ardakani, O.H., 2019, Mercury as a proxy for volcanic emissions in the geologic record: Earth-Science Reviews, v. 196, 102880, https://doi.org/10.1016/j.earscirev.2019.102880.

Hammarlund, E.U., Dahl, T.W., Harper, D.A., Bond, D.P., Nielsen, A.T., Bjerrum, C.J., Schovsbo, N.H., Schönlaub, H.P., Zalasiewicz, J.A., and Canfield, D.E., 2012, A sulfidic driver for the end-Ordovician mass extinction: Earth and Planetary Science Letters, v. 331, p. 128–139, https://doi.org/10.1016/j.epsl.2012.02.024.

Haq, B.U., and Schutter, S.R., 2008, A chronology of Paleozoic sea-level changes: Science, v. 322, p. 64–68, https://doi.org/10.1126/science.1161648.

Jablonski, D., 1991, Extinctions: A paleontological perspective: Science, v. 253, p. 754–757, https://doi.org/10.1126/science.253.5021.754.

Jones, D.S., Martini, A.M., Fike, D.A., and Kaiho, K., 2017, A volcanic trigger for the Late Ordovician mass extinction? Mercury data from south China and Laurentia: Geology, v. 45, p. 631–634, https://doi.org/10.1130/G38940.1.

Koehler, M.C., Stüeken, E.E., Hillier, S., and Prave, A.R., 2019, Limitation of fixed nitrogen and deepening of the carbonate-compensation depth through the Hirnantian at Dob's Linn, Scotland: Palaeogeography, Palaeoclimatology, Palaeoecology, v. 534, 109321, https://doi.org/10.1016/j.palaeo.2019.109321.

Kump, L.R., Arthur, M.A., Patzkowsky, M.E., Gibbs, M.T., Pinkus, D.S., and Sheehan, P.M., 1999, A weathering hypothesis for glaciation at high atmospheric pCO_2 during the Late Ordovician: Palaeogeography, Palaeoclimatology, Palaeoecology, v. 152, p. 173–187, https://doi.org/10.1016/S0031-0182(99)00046-2.

Lafargue, E., Marquis, F., and Pillot, D., 1998, Rock-Eval 6 applications in hydrocarbon exploration, production, and soil contamination studies: Revue de l'institut français du pétrole, v. 53, p. 421–437.

LaPorte, D.F., Holmden, C., Patterson, W.P., Loxton, J.D., Melchin, M.J., Mitchell, C.E., Finney, S.C., and Sheets, H.D., 2009, Local and global perspectives on carbon and nitrogen cycling during the Hirnantian glaciation: Palaeogeography, Palaeoclimatology, Palaeoecology, v. 276, p. 182–195, https://doi.org/10.1016/j.palaeo.2009.03.009.

Nardin, E., Godderis, Y., Donnadieu, Y., Le Hir, G., Blakey, R.C., Pucéat, E., and Aretz, M., 2011, Modeling the early Paleozoic long-term climatic trend: Geological Society of America Bulletin, v. 123, p. 1181–1192, https://doi.org/10.1130/B30364.1.

Nielsen, A.T., 2004, Ordovician sea level changes: A Baltoscandian perspective, *in* Webby, B.D., et al., eds., The Great Ordovician Biodiversification Event: New York, Columbia University Press, p. 84–93, https://doi.org/10.7312/webb12678-011.

Pogge von Strandmann, P.A.E., Desrochers, A., Murphy, M.J., Finlay, A.J., Selby, D., and Lenton, T.M., 2017, Global climate stabilisation by chemical weathering during the Hirnantian glaciation: Geochemical Perspectives Letters, v. 3, p. 230–237, https://doi.org/10.7185/geochemlet.1726.

Rong, J., Melchin, M., Williams, S.H., Koren, T.N., and Verniers, J., 2008, Report of the restudy of the defined global stratotype of the base of the Silurian System: Episodes, v. 31, p. 315–318, https://doi.org/10.18814/epiiugs/2008/v31i3/005.

Schmidt, A., et al., 2016, Selective environmental stress from sulphur emitted by continental flood basalt eruptions: Nature Geoscience, v. 9, p. 77–82, https://doi.org/10.1038/ngeo2588.

Scotese, C.R., and McKerrow, W.S., 1990, Revised world maps and introduction, *in* McKerrow, W.S., and Scotese, C.R., eds., Palaeozoic Palaeogeography and Biogeography: Geological Society of London Memoir 12, p. 1–21, https://doi.org/10.1144/GSL.MEM.1990.012.01.01.

Sepkoski, J.J., Jr., 1981, A factor analytic description of the Phanerozoic marine fossil record: Paleobiology, v. 7, p. 36–53, https://doi.org/10.1017/S0094837300003778.

Sheehan, P.M., 1973, The relation of Late Ordovician glaciation to the Ordovician-Silurian changeover in North American brachiopod faunas: Lethaia, v. 6, p. 147–154, https://doi.org/10.1111/j.1502-3931.1973.tb01188.x.

Shen, J., Algeo, T.J., Chen, J., Planavsky, N.J., Feng, Q., Yu, J., and Liu, J., 2019, Mercury in marine Ordovician/Silurian boundary sections of South China is sulfide-hosted and non-volcanic in origin: Earth and Planetary Science Letters, v. 511, p. 130–140, https://doi.org/10.1016/j.epsl.2019.01.028.

Smolarek-Lach, J., Marynowski, L., Trela, W., and Wignall, P.B., 2019, Mercury spikes indicate a volcanic trigger for the Late Ordovician mass extinction event: An example from a deep shelf of the peri-Baltic region: Scientific Reports, v. 9, 3139, https://doi.org/10.1038/s41598-019-39333-9.

Tribovillard, N., Algeo, T.J., Lyons, T., and Riboulleau, A., 2006, Trace metals as paleoredox and paleoproductivity proxies: An update: Chemical Geology, v. 232, p. 12–32, https://doi.org/10.1016/j.chemgeo.2006.02.012.

Wedepohl, K.H., 1995, The composition of the continental crust: Geochimica et Cosmochimica Acta, v. 59, p. 1217–1232, https://doi.org/10.1016/0016-7037(95)00038-2.

Williams, S.H., 1988, Dob's Linn—The Ordovician-Silurian boundary stratotype: Bulletin of the British Museum (Natural History): Geology Series, v. 43, p. 17–30.

Zhou, L., Algeo, T.J., Shen, J., Hu, Z., Gong, H., Xie, S., Huang, J., and Gao, S., 2015, Changes in marine productivity and redox conditions during the Late Ordovician Hirnantian glaciation: Palaeogeography, Palaeoclimatology, Palaeoecology, v. 420, p. 223–234, https://doi.org/10.1016/j.palaeo.2014.12.012.

Printed in USA